J Mater Sci (2007) 42:2643–2651
DOI 10.1007/s10853-006-1355-2

Chemical interaction between Crofer 22 APU and mica-based gaskets under simulated SOFC conditions

F. Wiener · M. Bram · H.-P. Buchkremer · D. Sebold

Received: 29 November 2005 / Accepted: 1 March 2006 / Published online: 4 January 2007
© Springer Science+Business Media, LLC 2006

Abstract Mica gaskets and also composite gaskets containing compressive mica interlayers are under consideration as sealing materials in solid oxide fuel cells (SOFC). To study potential interactions between the interconnect steel Crofer22APU and the mineral phases vermiculite (exfoliated) $(K,Mg,Fe)_3(Si,Al)_4O_{10}(OH)_2$ and talc $(Mg_3Si_4O_{10}(OH)_2)$, corrosion experiments were conducted in simulated SOFC conditions. The opposite walls of the gaskets were simultaneously exposed to air and wet H_2. A substantial increase in the thickness of the oxide layers formed by the interconnect steel is observed with specimen containing talc. The $Cr_2O_3/(Cr,Mn)_3O_4$ duplex layer normally formed on the Crofer is replaced by a thicker (factor of 5–10) layer of a complex microstructure that is assumed to contain Cr_2O_3, $(Cr,Mn,Mg,Fe)_3O_4$ and Fe_2O_3 phases. The modified microstructure is found in the entire air manifold, with an increased thickness up to a distance of 300 μm from the mica. It is proposed that magnesium is the critical component responsible for the accelerated oxide formation. A decomposition of talc is observed, which is discussed as the mechanism for the release of magnesium.

F. Wiener (✉) · M. Bram · H.-P.Buchkremer · D. Sebold
Institute for Materials and Processes in Energy Systems, IWV, Forschungszentrum Jülich GmbH, Leo-Brandt-Str., 52425 Jülich, Germany
e-mail: florian_wiener@yahoo.com

Introduction

SOFCs are used for energy conversion since they generate electrical power by the electrochemical reaction of an oxidant and a fuel gas. Currently two basic designs for SOFC applications exist: tubular and planar. Stacks of planar SOFCs are believed to offer the potential for higher cost efficiency, and higher power density per volume or mass when compared to tubular designs. However, a high temperature sealing concept ensuring stability and low leakage during long-term operation with thermal cycles remains a crucial challenge. An increase in leak rates reduces the efficiency of the system. Furthermore, larger leaks lead to gas-phase oxidation of the fuel, forming so-called ''hot spots.'' These can potentially damage SOFC stack components.

Gaskets in SOFC stacks need to fulfill a variety of requirements [1]. Long-term stable separation of oxidant and fuel gases has to be achieved. The seal has to maintain integrity through thermal cycling operation either by compensating or by tolerating mechanical and thermal mismatches of the stack components. The gasket materials need to withstand oxidizing and humid reducing atmospheres without degradation at an operating temperature of typically 1,073 K for several thousand hours. Also the seals should not degrade the materials they are in contact with nor form volatile compounds with the potential for electrode poisoning. Electrical insulation is required for designs with metallic interconnects to avoid short circuiting.

Currently glass-ceramics are the sealing material used most commonly. They offer gas tightness, and the potential for adaptation to the coefficient of thermal

expansion (CTE) of other stack components by controlling the crystallized phase content. Typically the electrical resistance and chemical inertia of glass-ceramics are sufficient for this application. However, due to the inherent brittleness and the rigid interfaces, crack growth in the sealant or the sealant/interconnect interface may occur during thermal cycling operation [2–4].

To overcome the drawbacks of rigid bonding of sealant materials with the interconnect or electrolyte, work began on developing a compressive sealing concept suitable for SOFC temperatures and the available sealing force [5–8]. Compressive seals based on mica show a high potential for SOFC applications. A novel composite seal with a sandwiched arrangement of functional layers has been developed by us [7]. In this design, shown in Fig. 1, the metallic gasket is supported by a compressive interlayer. Optionally, an electrically insulating layer is provided.

On simple geometries (50*50 mm square gaskets) it has been demonstrated that such a design has the potential to fulfill the requirements for SOFC sealing with respect to leak rates and insulating behavior [9]. Characteristic values for leak rates of 2 mica papers, the composite gasket without insulation, and the composite gasket with XJ766 as insulation are normalized over the gaskets inner circumference and summarized in Table 1.

The values are in good agreement with related investigations published recently [1]. The composite gasket advantageously combines the low leakage of metallic seals with the elastic recovery of the mica interlayer. From measurements on pure Thermiculite 815 an elastic recovery of at least 4.6% is expected [9].

The mica papers used as a compressive layer consist of minerals that contain alkaline and earth alkaline elements. It is claimed that some of these elements (Na, K) interact with Cr_2O_3—forming ferritic interconnect steels by accelerating chromium evaporation through volatile phases [10]. Accelerated rates of chromium evaporation pose two critical dangers. Cr impurities in the LSM or LSCF cathodes show a detrimental effect on the catalytic activity of the cathode material [11]. This cathode poisoning potentially affects system aging rates by orders of magnitude. Furthermore, a depletion of the Cr content below a threshold value of 16 at.% causes catastrophic breakaway oxidation in Crofer.

In this paper, the influence of talc on oxide scale growth of the interconnect material Crofer 22 APU is investigated. Potential consequences of these interactions on the continuous operation of SOFC stack are discussed.

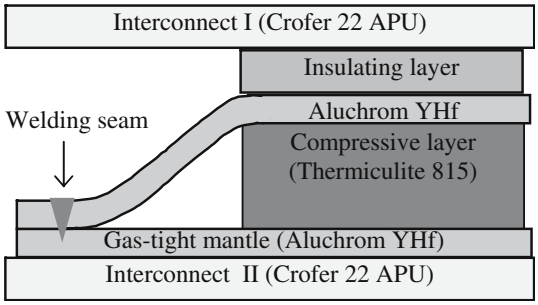

Fig. 1 Scheme of the composite gasket (cross-section). Functional layers and materials used are indicated

Table 1 Leak rates of mica papers and the composite gasket (2 layers Aluchrom YHf, Thermiculite 815) at 1,073 K. The gas pressure difference is 20 kPa, compressive stress 0.68 MPa

Gasket	Leak rate (sccm cm^{-1})
Thermiculite 815	$4*10^{-1}$
Thermiculite XJ766	$2*10^{-2}$
Composite gasket	$1*10^{-2}$
Composite gasket, insulating interlayer	$3*10^{-2}$

Experimental

Corrosion experiments were conducted on two gaskets placed between sheets of the ferritic alloy Crofer 22 APU/1.4760 (Thyssen VDM, Germany). Both gaskets had a square shape with 50 mm outer length. The width of the sealing face was 4 mm. One gasket was cut from pure Thermiculite XJ 766 mica paper (Flexitallic, UK) and precompressed to 300 μm thickness with 30 kN force. The second gasket consisted of a welded mantle of two sheets of Aluchrom Yhf/1.4767 (Thyssen VDM), thickness 230 μm, encapsulating a layer of Thermiculite 815 (Flexitallic, UK) mica (with a 100 μm 316 L inlay) precompressed to 800 μm thickness. Thermiculite XJ766 was used as an insulating interlayer. Figure 2 shows a photograph of the sample used for the

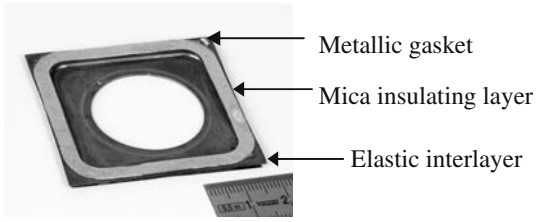

Fig. 2 Photograph of 1st generation composite gasket used for determination of leak rates

subsequent investigation. The absolute thickness of the composite gasket was 1.56 mm.

Thermiculite 815 consists of exfoliated vermiculite ($(K,Mg,Fe)_3(Si,Al)_4O_{10}(OH)_2$) while Thermiculite XJ766 is a mixture of vermiculite and talc ($Mg_3Si_4O_{10}(OH)_2$). The cation content of both mica papers in the as-received state was determined by inductively coupled plasma optical emission spectroscopy (ICP-OES).

The procedure for simultaneous corrosion testing in reducing and oxidizing atmospheres is described in detail in [12]. The testing was conducted for 400 h at 1,073 K with air in one manifold and with hydrogen with 3 vol.% H_2O in the other. A scheme of the setup is shown in Fig. 3.

After the corrosion test, cross sections of the gaskets were prepared for SEM/EDX (Zeiss, Gemini 1530) to analyze the morphology and chemical composition (qualitative) of the samples.

Another test was conducted to determine weight loss and to prepare samples for XRD and chemical analysis by ICP-OES. Therefore air was passed over a sample of 1.142 g Thermiculite XJ766 in a tube furnace at 1,073 K for 400 h at a rate of 3,000 sccm min^{-1}.

The phase content of this sample before and after treatment was determined by XRD on a powder diffractometer (Siemens, D500).

Simultaneous DTA/TG (Netzsch, STA 409C) was performed on as-received Thermiculite XJ766. Ramps of 5 K min^{-1} were used with holding times of 60 min at 1,073 K and 1,223 K. The dwell temperature of 1,073 K corresponds to SOFC operating conditions at the research center Juelich, 1,223 K is the upper application limit for Thermiculite.

Results and discussion

Interactions between the gasket material and the interconnect steel are most clearly manifested in compositional and morphological changes of the oxide scales formed on the metal. The Crofer 22 APU interconnect steel was developed to form a duplex-oxide layer [13]. On top of the protective Cr_2O_3 layer, a stable $(Cr,Mn)_3O_4$-spinel is assumed to inhibit chromium evaporation from the chromia scale. Overall thickness of both layers after 400 h is generally 2–3 μm on the air side and 1–2 μm on the fuel side. For future reference, a cross-sectional view of the surface of this steel (1.4760) after 250 h at 1,073 K in air is shown in Fig. 4. A galvanic Ni coating was used for this sample preparation.

Characterization of the Thermiculite XJ766 gasket

The changes of morphology and phase content of the oxide scales on the interconnect steel in contact with mica paper under air and wet hydrogen are compared in Fig. 5. Figure 5f indicates the location of the investigated sample areas. Table 2 summarizes the observed phase content.

On the air side in direct contact with the mica an area of increased oxide thickness (20–25 μm) extending up to a distance of 250–300 μm from the gasket is formed (Fig. 5a). The dense oxide displays an obvious layer sequence: A $Cr(Cr,Mn,Fe)_3O_4$ of thickness <5 μm with an unusually low concentration of Mn is formed directly on the Crofer 22 APU interconnect material. Then a strip of iron-rich chromium oxide follows. The top layer is a 15–20 μm thick, homogeneous region of Cr oxide, with significant amounts of

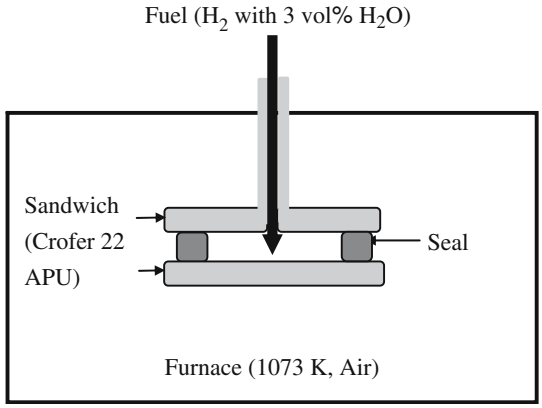

Fig. 3 Scheme of sample in the test-bed for simulated SOFC environment. H_2 lost through leakage is constantly replaced

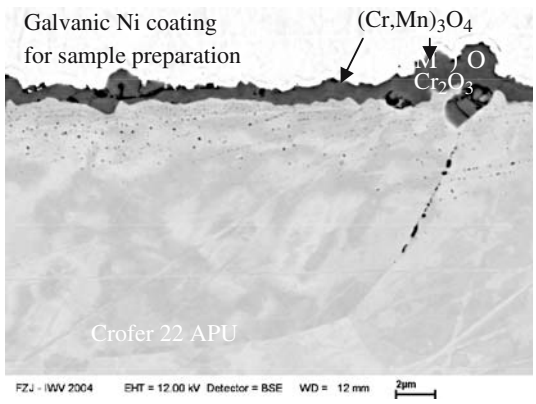

Fig. 4 Duplex oxide morphology of Crofer22 APU/1.4760 after 250 h at 1,073 K

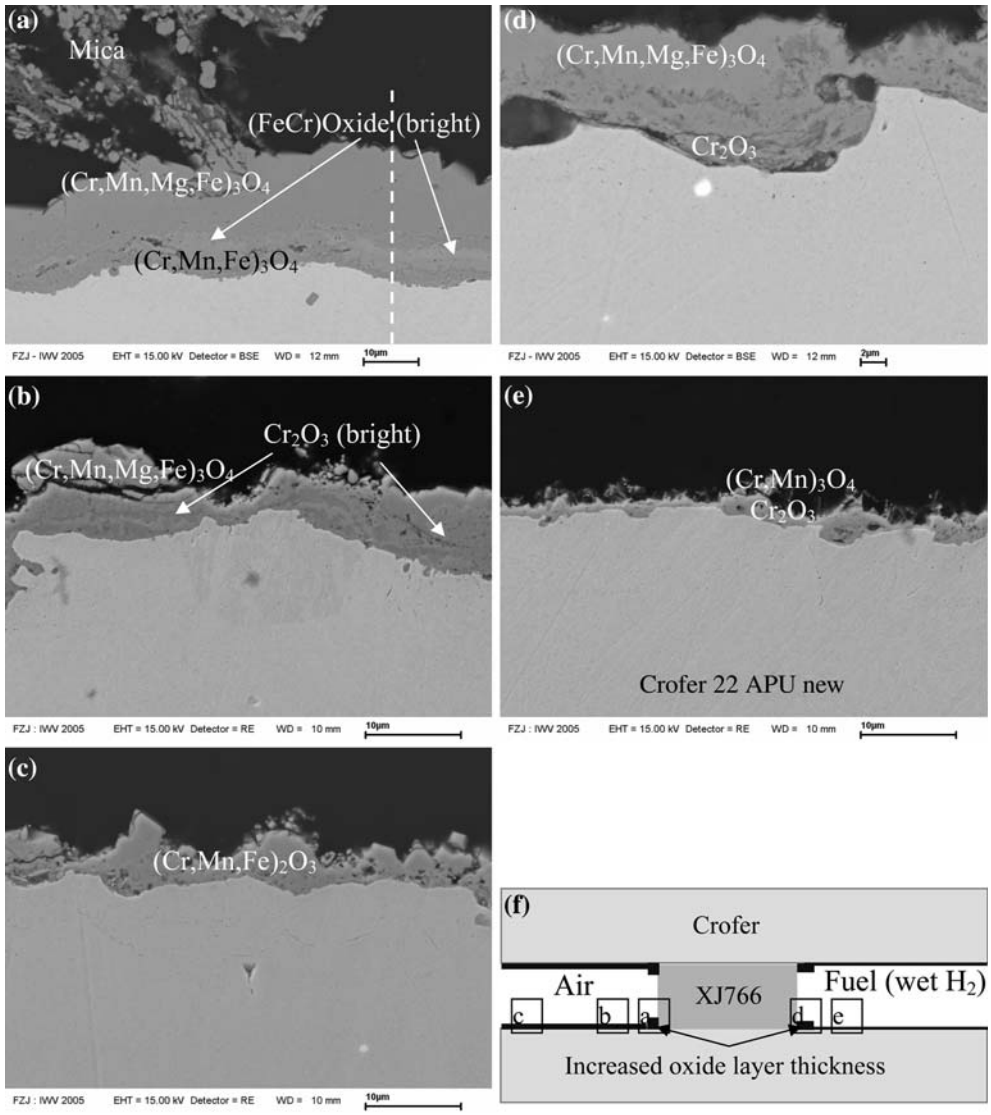

Fig. 5 Overview of findings in gasket A (XJ766)) after 400 h at 1,073 K. (**a**) air manifold, contact area. The dashed line shows the position of Fig 6; (**b**) air manifold, 500 μm distance from mica; (**c**) air manifold, 3,800 μm distance; (**d**) fuel manifold, contact area; (**e**) fuel manifold, 500 μm distance; (**f**) overview

Table 2 Phase content of the oxide scales at different sample areas after heat treatment at 1,073 K/400 h

Arranged according to increasing distance from interconnect

Manifold, figure	Distance from mica (μm)	Assumed phase content	Total thickness of oxide scale (μm)
Air, 5a	0	$(Cr,Fe,Mn)_3O_4$, (Fe,Cr)-oxide, $(Cr,Mn,Mg,Fe)_3O_4$	20–25
Air, 5b	500	Two phases, mixed, $Cr_{1.9}(Mn,Mg,Fe)_{1.1}O_4$, Cr_2O_3	3–5
Air, 5c	3800	Single phase oxide with $Cr_{0.94}$ $(Mn,Fe)_{0.06}$	3–5
Fuel, 5d	0	Duplex Cr_2O_3, $Cr_{2.3}(Mn,Mg,Fe)_{0.7}O_4$	8–10
Fuel, 5e	500	Duplex Cr_2O_3, $(Cr,Mn)_3O_4$	1–2

Mg, Fe and Mn. In this oxide Mn clearly shows enrichment towards the air manifold, whereas for Fe and Mg no obvious gradient exists. However, there is a sharp peak of Mg at the interface with air. For clarity the linescan of Mn and Mg indicated in Fig. 5a is shown in Fig. 6.

The EDX-linescan was continued inside the Crofer 22 APU steel up to a depth of 195 μm to investigate whether the formation of the abnormal oxide scale is accompanied by Cr depletion (Table 3).

The obvious decrease of Cr (18.2 wt.%) towards the interface enhances the risk of catastrophic oxidation as evident from the formation of unstable Fe-containing oxides. The area shown in Fig. 5a is the only position in the sample where a clear Cr depletion was found.

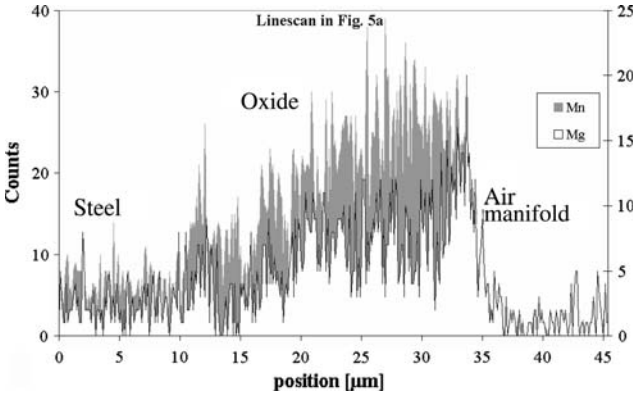

Fig. 6 EDX linescan for Mg and Mn in Fig. 5a. An increased Mg content in contact with air is evident

Table 3 Chromium concentration in Crofer 22 APU interconnect underneath thick oxide scales in the air manifold, determined by EDX

Distance from oxide (μm)	Cr (wt.%)
6	18.2
27	19.5
48	21.9
69	23.1
90	23.8
111	24.6
132	24.5
153	23.8
174	23.6
195	23.8

The position of the line scan is shown in Fig. 5a

Figure 5b and c shows the oxide scale taken at a distance of 500 μm and 3800 μm, respectively. Neither of these structures is as developed as in the reference (Fig. 4). The reference shows a clearly layered arrangement of duplex oxides: A strip of pure Cr_2O_3 on the metal, and a top layer of $(Cr,Mn)_3O_4$. As usual with polycrystalline materials the oxides scale on the grain boundaries shows a slightly different morphology. In the investigated sample, at a distance of 500 μm the scale separates into two phases (Fig. 5b), which can be distinguished by phase contrast. The brighter phase, almost pure Cr_2O_3, is embedded in a matrix of (Cr,Mn,Mg,Fe) oxide, which is most likely a solid-solution spinel of composition $Cr_{1.9}(Mn,Mg,Fe)_{1.1}O_4$. The relative error of the elemental distribution determined with EDX is 5%.

The oxide scale at a distance of several mm from the gasket shows a somewhat increased thickness (3–5 μm) and fails to develop a layered duplex morphology. Instead, a single oxide phase with 94% Cr and 6% (Mn + Fe) content is observed (Fig. 5c). The Mn concentration of this phase is homogeneous, but at a

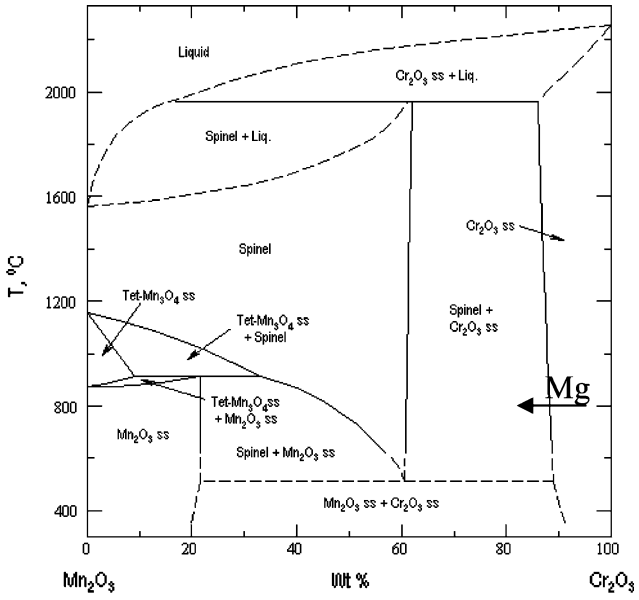

Fig. 7 System Mn_2O_3–Cr_2O_3 in air. Of particular interest is the phase boundary at 90% Cr_2O_3 at 1,073 K

significantly lower level than the spinel phase of the reference sample. The phase diagram for the system Cr_2O_3–Mn_2O_3 (Fig. 7) was originally published in [14] and is included in the database [15]. It suggests Cr_2O_3 containing Mn and Fe in solid solution.

On the fuel side, the oxide thickness increases to 8–10 μm in direct contact with the mica (Fig. 5d). Under anode conditions, the microstructure remains a layered duplex. Mg is detected in the spinel (about $Cr_{2.3}(Mn,Mg,Fe)_{0.7}O_4$, but not in Cr_2O_3. This area of increased oxide growth extends 400 μm starting from the edge of the mica.

At distances of more than 400 μm, the oxide scale exhibits the usual morphology and composition as known from the reference samples under anode conditions.

Chemical analysis, DTA/TG and XRD on Thermiculite XJ766

The chemical analysis for both investigated mica materials is shown in Table 4, the results of the thermal analyses are given in Fig. 8.

No statistically significant change in the chemical analysis before and after heat-treatment was observed. An overall loss of 6 wt.% was measured. The material continuously loses around 3% of mass from 953 K to 1,098 K, the majority at the holding temperature of 1,073 K. A sharp decrease is observed at 1,098 K during further heating. The mica rapidly loses 2.2 wt.% in a narrow temperature range. No further weight loss

Table 4. Chemical analysis of Thermiculite 815 and Thermiculite XJ 766 by ICP-OES (wt.%).

	Thermiculite 815 as received	Thermiculite XJ766 as received	Thermiculite XJ766 after heat treatment
Si	22.8	26.5	25.3
Al	4.8	3.6	3.5
Ti	0.68	0.56	0.55
Fe	5.5	3.9	3.8
Na	0.64	0.22	0.21
K	4.8	2.3	2.1
Mg	15.7	14.8	15.4
Ca	0.82	0.50	0.50
Ba	0.10	0.11	0.10
Cr	–	–	0.068
Mn	–	–	0.046

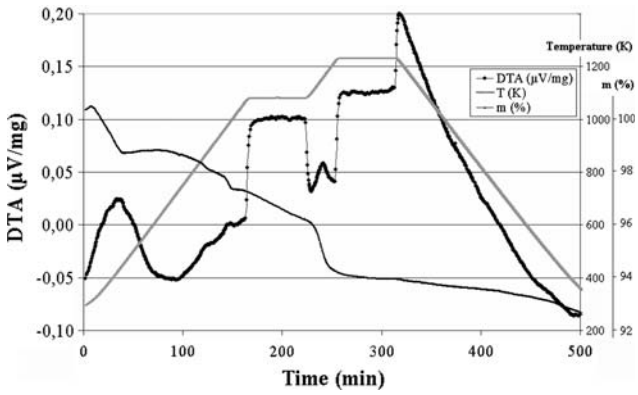

Fig. 8 DTA/TG with ramps of 5 K min^{-1} on Thermiculite XJ766. The decomposition of talc starts at 950 K

is observed at the final holding temperature of 1,223 K. DTA reveals two exothermic peaks at 1,083 K and 1,213 K.

The sample treated in a tube furnace for 400 h at 1,073 K showed an overall mass loss of 7.3 wt.%. As usual with Thermiculite XJ766 embrittlement is observed.

The dissociation of talc to enstatite ($MgSiO_3$), SiO_2 and H_2O with a mass loss of 4.7 wt.% is reported to take place at 1,023–1,073 K [16]. To verify the phase content of as-received Thermiculite XJ766, and to investigate the phase equilibrium after 400 h at 1,073 K under atmospheric conditions powder diffraction data were collected and are shown in Fig. 9.

In the starting material two minerals, vermiculite and talc, are evident. The majority of vermiculite exists as a "10 Å phase" [17], in this case partially exfoliated/dehydrated vermiculite with a d(001) spacing of 1–1.2 nm. Small amounts of hydrated vermiculite $(K,Mg,Fe)_3(Si,Al)_4O_{10}(OH)_2{*}4(H_2O)$ with d(001) spacing of 1.4 nm can also be confirmed.

The heat treated sample contains fully dehydrated vermiculite, quartz and enstatite without evidence of talc or 1.4 nm vermiculite. The peaks labeled V10 were confirmed by calculation of a monoclinic lattice with $a = 0.53$ nm, $b = 0.92$ nm, $c = 1.02$ nm, $\beta = 95°$. Thus during the heat-treatment the remaining water was removed from vermiculite, while talc decomposed to enstatite and quartz following the reaction.

$$Mg_3Si_4O_{10}(OH)_2 \rightarrow 3MgSiO_3 + SiO_2 + H_2O \quad (1)$$

which proceeded completely under the given conditions.

Characterization of the composite gasket

The investigation of the second sample, the composite gasket, yields similar observations. As an example, two micrographs from the air manifold are shown in Fig. 10. Figure 10a shows an overview of the gasket on the air side, and Figure 10b a detailed image of the observed oxide scale of unusual composition and dimensions.

It is assumed that the presence of Thermiculite XJ766 modified the oxidation behavior of Crofer 22 APU. It is important to mention that an increased thickness of the oxide scale was observed on the upper interconnect, indicating the occurrence of volatile constituents from the mica.

Apparently, the mica does not influence the formation of aluminum oxide scales on the Aluchrom YHf used in the composite gasket, while the 316 stainless steel core of the Thermiculite 815 is, unsurprisingly, strongly corroded.

Discussion of experimental observations

The presence of talc-containing Thermiculite XJ766 influences oxidation behavior strongly on the air side, and moderately on the anode manifold. The effect is most profound in the direct contact area interconnect/mica. This area shows an oxide thickness of 20–25 µm, mainly consisting of $(Cr,Mn,Mg,Fe)_3O_4$. Chromium depletion of the Crofer 22 APU steel is evident. At distances of more than 500 µm from the mica no significant increase of oxide scale thickness is observed, but the material fails to develop a protective duplex layer.

On the fuel side, the usual duplex layer is developed. At areas in direct contact with mica, Mg is detected in the top layer, the spinel. The thickness of the scale increases to 8–10 µm, while no iron in the oxide nor chromium depletion of the steel have been determined.

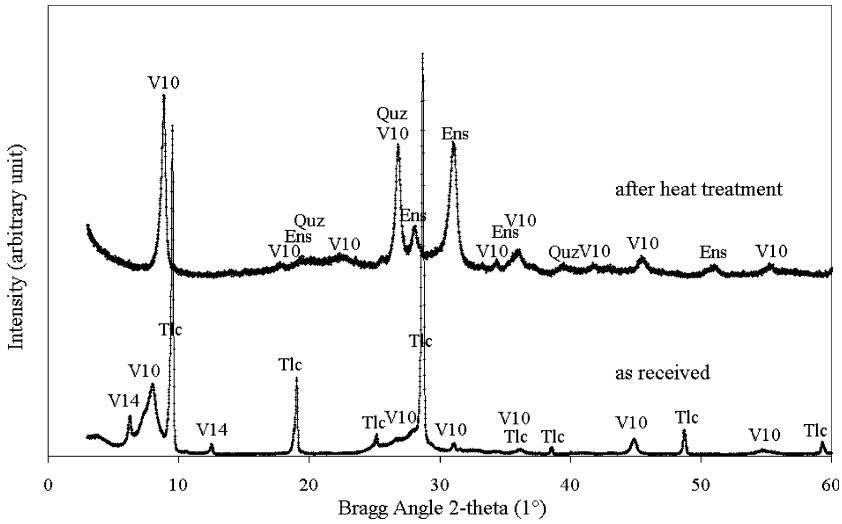

Fig. 9 XRD (Cu-$K_{\alpha 1}$, 2-theta 5–60°) on Thermiculite XJ766 as received and after heat treatment (1,073 K, 400 h) reveals the complete decomposition of talc. Tlc: talc; V10: dehydrated vermiculite; V14: hydrated vermiculite, Ens: enstatite; Quz: quartz

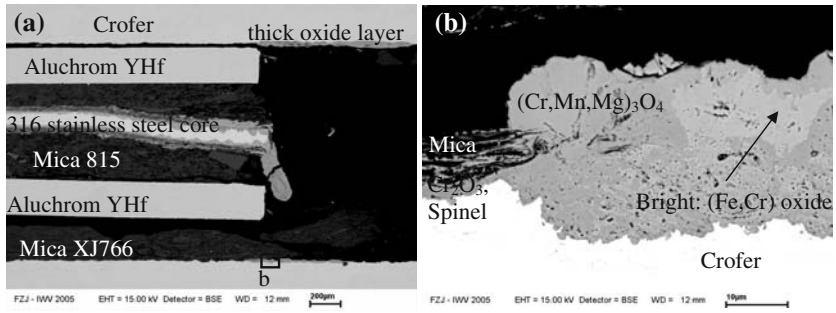

Fig. 10 Overview of findings in gasket B (composite gasket with insulating interlayer) after 400 h at 1,073 K. Increased oxide scale thickness is evident on Crofer not in direct contact with mica. This indicates a gas-phase transport mechanism

On both sides, Mg can be detected in the oxides whose morphology is unusual. Na and K are contained at low concentrations in the as-received mica materials, but cannot be detected in the oxide scale.

The dissociation of talc with the evolution of water is shown in XRD and DTA/TG data. Vermiculite remains stable under SOFC conditions. Thus, Thermiculite 815 is preferred regarding its chemical stability, but has to be ruled out because of high leak rates (Table 1).

The microstructural investigations point towards Mg as the main cause of modified oxidation behavior. The evidence of Mg in oxide scales far from the source (Fig. 10, oxide on top) is evidence for a gas-phase transport mechanism. A likely cause of the Mg mobilization is the decomposition reaction of talc(1).

Apparently the reaction is a simple unit cell transformation between the unit cell of talc $Mg_3Si_4O_{10}(OH)_2$ with $a = 0.529$ nm, $b = 0.916$ nm, $c = 1.870$ nm and enstatite $MgSiO_3$ with $c = 0.518$ nm, $b = 0.881$ nm, $a = 1.823$ nm [18]. According to a review [19] it follows that one unit cell of talc contains the following number of atoms: 16 Si, 12 Mg, 48 O, 8 H, whereas enstatite comprises 16 Si, 16 Mg, 48 O. To maintain charge balance the 8 protons lost from the talc unit cell during dehydroxilation are replaced by counter-migration of 4 Mg. The regions thus depleted of Mg form SiO_2. The described process requires very slight movement of the cations in the $Mg(OH)_2$ layer, the octahedral sheet in the talc structure. In the same paper other authors describe the formation of free MgO and SiO_2, especially at lower temperatures. Together with the water evolved from the reaction, the formation of intermediate compounds (e.g., $Mg(OH)_2$) appears feasible. $Mg(OH)_2$ readily decomposes to MgO which is evident on the contact area air/oxide scale in Fig. 6.

From this reservoir of Mg, incorporation into the oxide (spinel) scale is not unexpected from the study of phase diagrams for the oxides of Fe, Cr, Mn and Mg under the experimental conditions [15]. Conditions on the air side are 1,073 K with an oxygen partial pressure $p(O_2)$ of 21 kPa. The $p(O_2)$ on the fuel side is determined by the H_2/H_2O equilibrium and amounts to $4.1*10^{-17}$ Pa. Generally, the oxides of Fe, Cr, Mg and Mn show a tendency to form solid solutions with each other. This is due to similar ionic radii of the constituents, and the isomorphism of the corundum type at high $p(O_2)$ or the spinel-type at lower $p(O_2)$.

Table 5 Effective cystal radii of selected oxides [18]

Ion	Coordination	Crystal radius (pm)
Cr^{2+}	VI	87*
Cr^{3+}	VI	75.5
Mg^{2+}	IV	71
Mg^{2+}	VI	86
Mn^{2+}	IV	66
Mn^{2+}	VI	81*
Mn^{3+}	VI	72

*Indicates low-spin state

The phase equilibria diagrams published by AcerS-NIST are used as a reference [15]. From the binary phase diagrams for Cr_2O_3–Mn_2O_3 (2133), MgO–Cr_2O_3 (262) and MgO–MnO (6,737) it is established that spinel solid solutions are formed at 1,073 K if the Mg or Mn concentration exceeds 10%. The similar crystal radii for Mn^{2+} and Mg^{2+} (Table 5) in tetrahedral coordination [20] would indicate the possibility that a solid solution could form in the respective oxides.

Since no published data for the ternary system Cr_2O_3–Mn_2O_3–MgO exists, diagram 2,133 (Fig. 7) is considered, with Mg^{2+} replacing some of the Mn.

At 1,073 K, single phase Cr_2O_3 with Mn in solid solution (ss) exists as long as the Cr_2O_3 concentration exceeds 90%. At chromia concentrations from 60% to 90% phase separation into Cr_2MnO_4 and Cr_2O_3 ss occurs. From the EDX data it appears that the Mg concentration increases towards the mica gasket. It is proposed that the single phase oxide far from the mica is a Cr_2O_3 ss containing Mn. The phases in the areas richer in Mg are $(Cr,Mn,Mg)_3O_4$ and Cr_2O_3.

In the reference sample, such behavior is not observed. The oxide scale contains an equivalent amount of Mn, while overall volume is smaller. Thus the Mn concentration is higher, and the Cr_2O_3 ss field in the phase diagram is not reached. Cr_2MnO_4 and Cr_2O_3 form in the typical sandwiched structure, following the $p(O_2)$ gradient between gas phase and bulk metal.

The high concentrations of Fe^{3+} in the oxide (chromia, spinel) scales at the triple point air/steel/mica point to the beginning of a catastrophic breakaway oxidation

Conclusions for stack operation and gasket development

The obvious deterioration of interconnect oxidation behavior is not tolerable. The formation of iron-containing oxides even after 400 h points to the possibility of catastrophic breakaway oxidation in operation. On the air side the absence of a duplex layer poses the danger of accelerated chromium evaporation and cathode poisoning. In the reference sample the outermost $(Cr,Mn)_3O_4$ immobilizes chromium, while the investigated samples contain less stable solid solutions of Mn, Mg and Fe in chromia.

The dissociation of the talc in Thermiculite XJ766 at temperatures below SOFC conditions is not tolerable for high-temperature SOFCs ($T \geq 1{,}023$ K). For intermediate temperature SOFCs (923 K) the material could potentially be used.

As a consequence for the next generation of the composite gasket a full encapsulation of the compressive mica interlayer is provided to reduce the risk of undesired volatile constituents. The application of electrically insulating interlayers (e.g., $MgAl_2O_4$, MgO) is pursued by PVD techniques.

Conclusions

Mica paper is discussed as a promising sealing material for SOFC stacks. To achieve low leakage rates, the use of talc as a filler phase is prerequisite. A test set-up where mica is exposed to a dual atmosphere simulating SOFC conditions reveals that the talc undergoes a complete phase transformation at SOFC operating temperatures of 1,073 K leading to the formation of volatile constituents. This results in a modification of ferritic steel corrosion. On the oxidant manifold Mg is incorporated into oxide scales, modifying an ordered duplex layer to a disordered microstructure. In the triple point of mica/steel/air the modified composition is accompanied by rapid oxide growth of iron-containing oxides, and chromium depletion in the steel.

Acknowledgements The authors would like to thank V. Haanappel for conducting the experiments in the simulated SOFC environment, and M. Kappertz for the metallographic preparation. We would like to thank W.J. Quadakkers and P. Huczkowski for reference micrographs and helpful discussions.

References

1. Fergus JW (2005) J Power Sour 147:46
2. Ley KL, Krumpelt M, Kumar R, Meiser JH, Bloom I (1996) J Mater Res 11:1489
3. Ohara S, Mukai K, Fukui T, Sakaki Y (2001) J Ceram Soc Jap 109:186
4. Lahl N, Singheiser L, Hilpert K, Singh K, Baradur D (1999) In: Electrochemical society proceedings, vol 99, p 1057
5. Chou Y-S, Stevenson JW, Chick LA (2003) J Am Ceram Soc 86:1003
6. Bram M, Reckers S, Drinovac P, Moench J, Steinbrech RW, Buchkremer HP, Stoever D (2003) Proc Electrochem Soc. 2003–2007 (SOFC VIII) 888

7. Bram M, Reckers S, Drinovac P, Moench J, Steinbrech RW, Buchkremer HP, Stoever D (2004) J Power Sour 138:111
8. Chou Y-S, Stevenson JW (2005) J Power Sour 140:340
9. Wiener F, Behr W, Bram M, Buchkremer HP, Steinbrech RW (2005) Poster presentation, 9th Grove Fuel Cell Symposium, London, UK
10. Weiß R, Peck D, Mille M, Hilpert K (1996) Proceedings of the 17th Risø International Symposium on Materials Science, Roskilde, Denmark, 1996, 479
11. Matzsuzaki Y, Yasuda I (2001) J Electrochem Soc 148:A126–A131
12. Haanappel VAC, Vinke IC, Wesermeyer H (2004) In: Proceedings of the 6th European SOFC Forum, Lucerne, Switzerland, 2004, 784
13. Huczkowski P, Shemet V, Piron-Abellan J, Singheiser L, Quadakkers WJ, Christiansen N (2004) Mater Corros 55:825
14. Speidel DH, Muan A (1963) J Am Ceram Soc 46:577
15. ACersS-NIST Phase Equilibria Diagrams, CD-ROM Database, Version 3.0.1
16. Bose K, Ganguly J (1995) Earth Planet Sci Lett 136:109
17. Fumagalli P, Stixrude L, Poli S, Snyder D (2001) Earth Planet Sci Lett 186:125
18. Wesolowsk M (1984) Thermochimica Acta 78:395
19. MacKenzie KJD, Meinold RH (1994) Thermochimica Acta 244:195
20. Shannon RD (1976) Acta Crystallogr A32:751